Supporting Information for:

Structural and functional analysis of parameters governing tankyrase-1 interaction with telomeric repeat-binding factor 1 and GDP-mannose 4,6-dehydratase

Travis Eisemann, Marie-France Langelier, and John M. Pascal

Table of Contents:

Figure S1: TRF1 and GMD mutant construct competition binding assays
Figure S2: Multimerization deficient TRF1 constructs
Figure S3: Multimerization deficient GMD constructs
Figure S4: TBM mutant Western blot images
Figure S5: Analytical ultracentrifugation analysis of TNKS-12345 and GMD complexes
Figure S6: Analytical ultracentrifugation analysis of TNKS-12345 and TRF1
Figure S7: TNKS:TRF1 solubility assays
Figure S8: TNKS binding partner solvent accessibility
Figure S9: NS-TNKS MARylation density for hydrolase time series
Table S1: Solvent accessibility of consensus and TNKS binding partner crystal structures

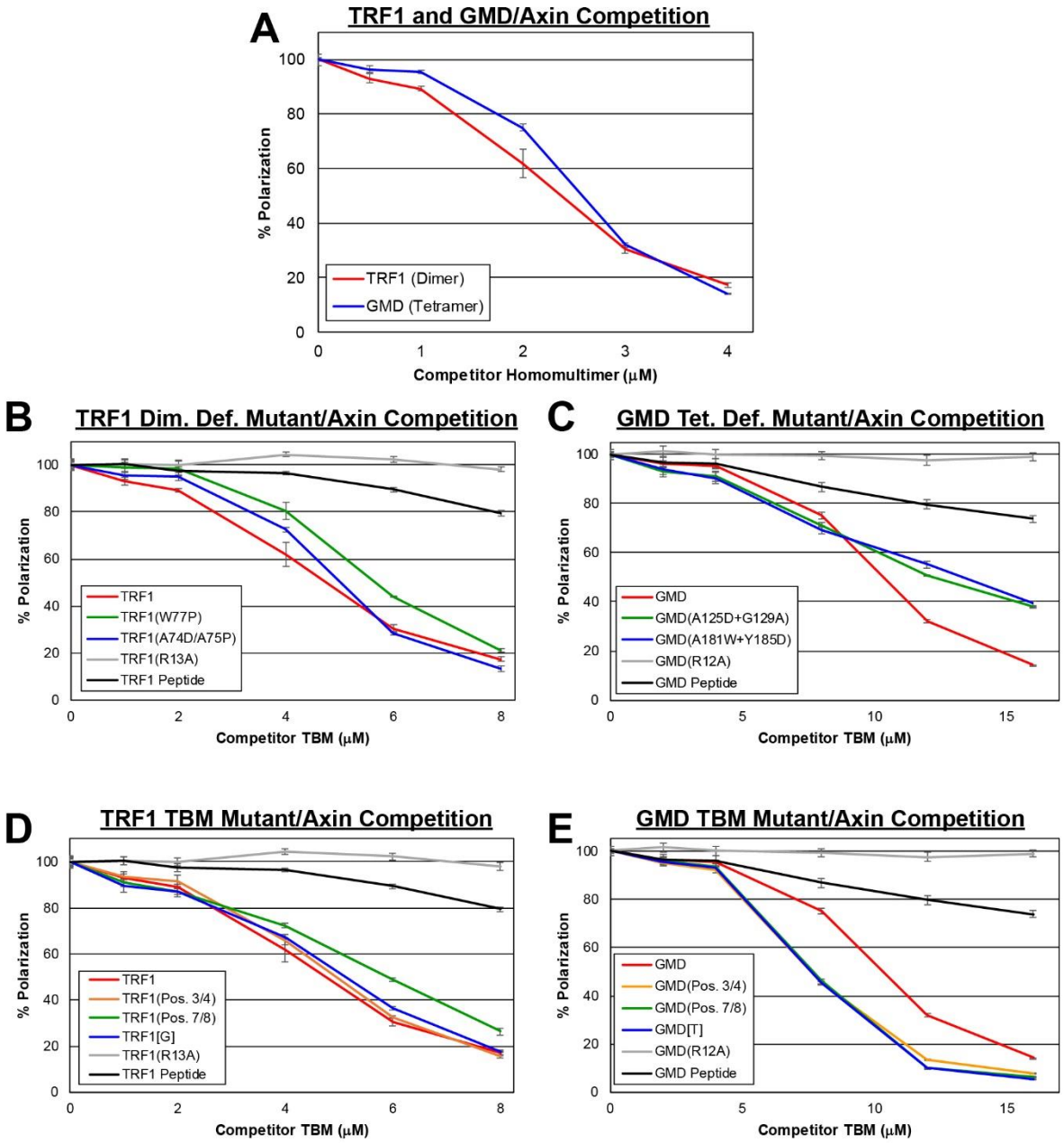

Figure S1. TRF1 and GMD mutant construct competition binding assays. (A) Competition fluorescence polarization assay measuring the competition between an Axin1 peptide and full-length TRF1 or GMD. Competitor concentrations represent homomultimers, with TRF1 as a dimer and GMD as a tetramer. (B and C) Competition assays measuring the effect of multimerization disruption on the ability of TRF1 (B) and GMD (C) to compete with an Axin1 peptide for TNKS binding. Competitor concentrations represent TRF1 and GMD monomers. Data represent mean ± standard deviation. (D and E) Competition assays measuring the effect of TBM mutation on the ability of TRF1 (D) and GMD (E) to compete with an Axin1 peptide for TNKS binding. Competitor concentrations represent TRF1 and GMD monomers. Data represent mean ± standard deviation.

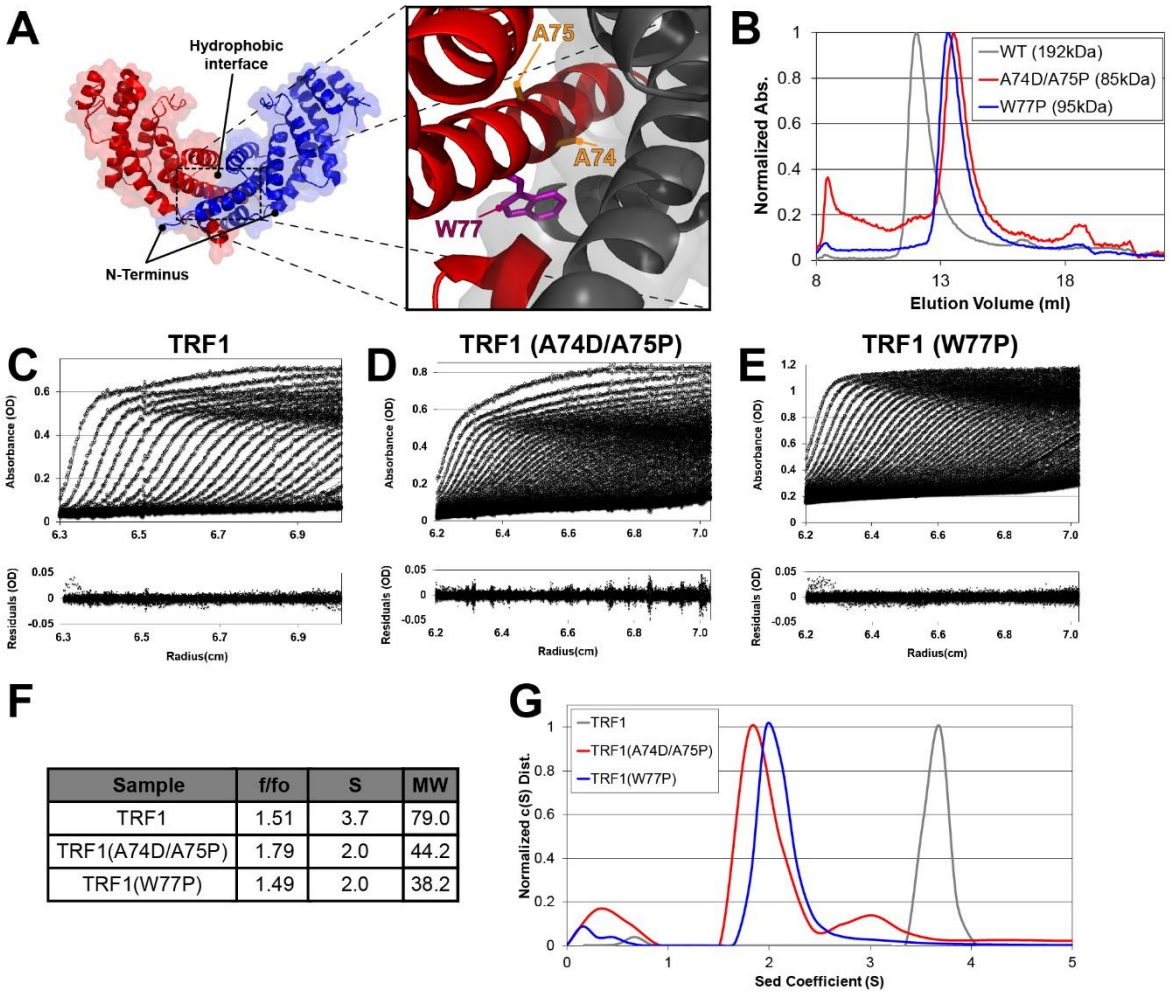

Sample	f/fo	S	MW
TRF1	1.51	3.7	79.0
TRF1(A74D/A75P)	1.79	2.0	44.2
TRF1(W77P)	1.49	2.0	38.2

Figure S2. Multimerization deficient TRF1 constructs. (A) Crystal structure of the TRF1 dimerization domain (PDB # 1H6O). Mutagenesis targets A74/A75 (orange) and W77 (purple) are shown (box). (B) Analytical gel filtration analysis of TRF1 dimerization deficient mutants compared to wild type TRF1. Approximate molecular weights are indicated in the legend. (C-G) Sedimentation velocity analysis (C-E), sedimentation parameters (F) and c(S) distribution (G) of wild type TRF1 and dimerization deficient TRF1 mutants. The top panels show absorbance data (circles) and associated c(S) model fit (lines). The bottom panels show residual for the fit. TRF1 was loaded at 6.95 µM (0.7 mg/ml) (dimer concentration, 13.9 µM monomer). TRF1(W77P) and (A74D/A75P) were loaded at 13.6 µM and 11.9 µM (monomer concentration, or 0.68 mg/ml and 0.60 mg/ml), respectively.

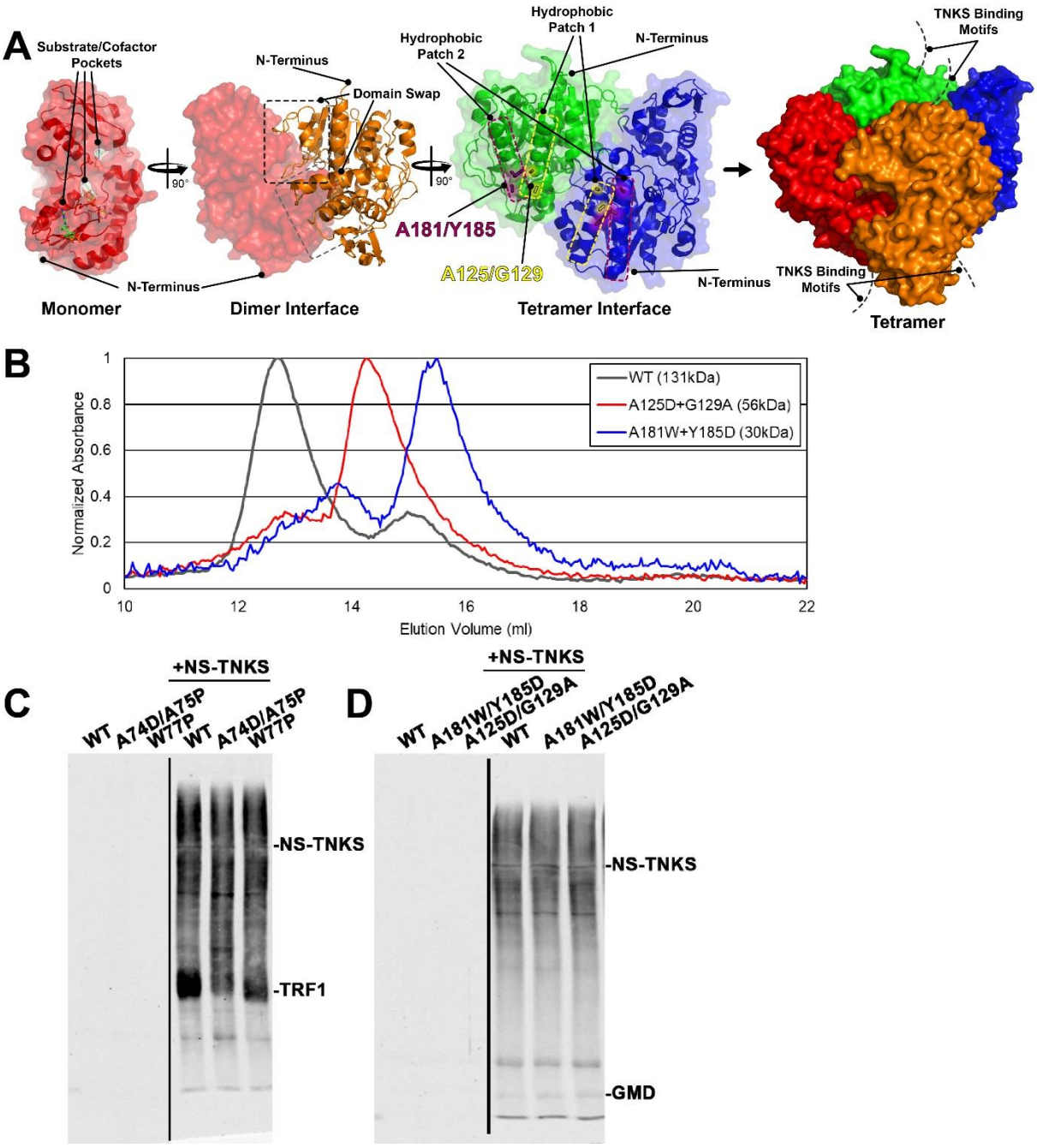

Figure S3. Multimerization deficient GMD constructs. (A) Schematic depicting the dimerization and tetramerization interfaces of a crystal structure of GMD (PDB # 5IN5). Tetramerization-deficient mutagenesis targets in Patch 1, A125/G129 (yellow), and Patch 2, A181/Y185 (purple), are shown. (B) Analytical gel filtration analysis of GMD dimerization deficient mutants compared to wild type GMD. Approximate molecular masses are indicated in the legend. (C and D) Western blots for TNKS activity assays using TRF1 (C) and GMD (D) multimerization deficient mutants. The black dividing line represents where the blots were sliced for presentation purposes.

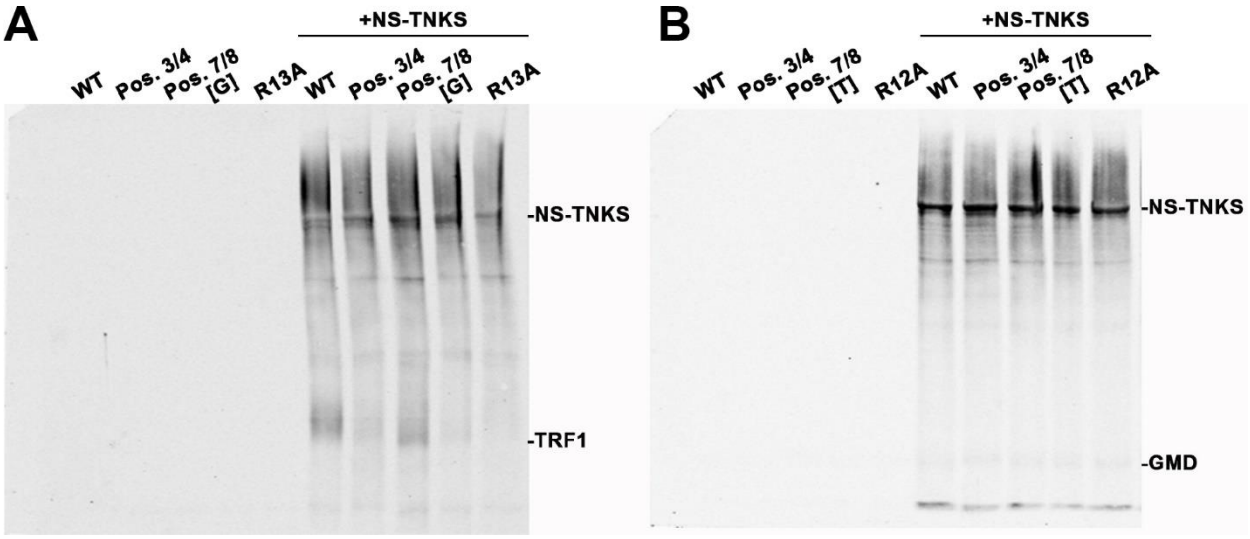

Figure. S4. TBM mutant Western blot images. (A and B) Western blot images for TNKS activity assays using TRF1 (A) and GMD (B) TBM mutants.

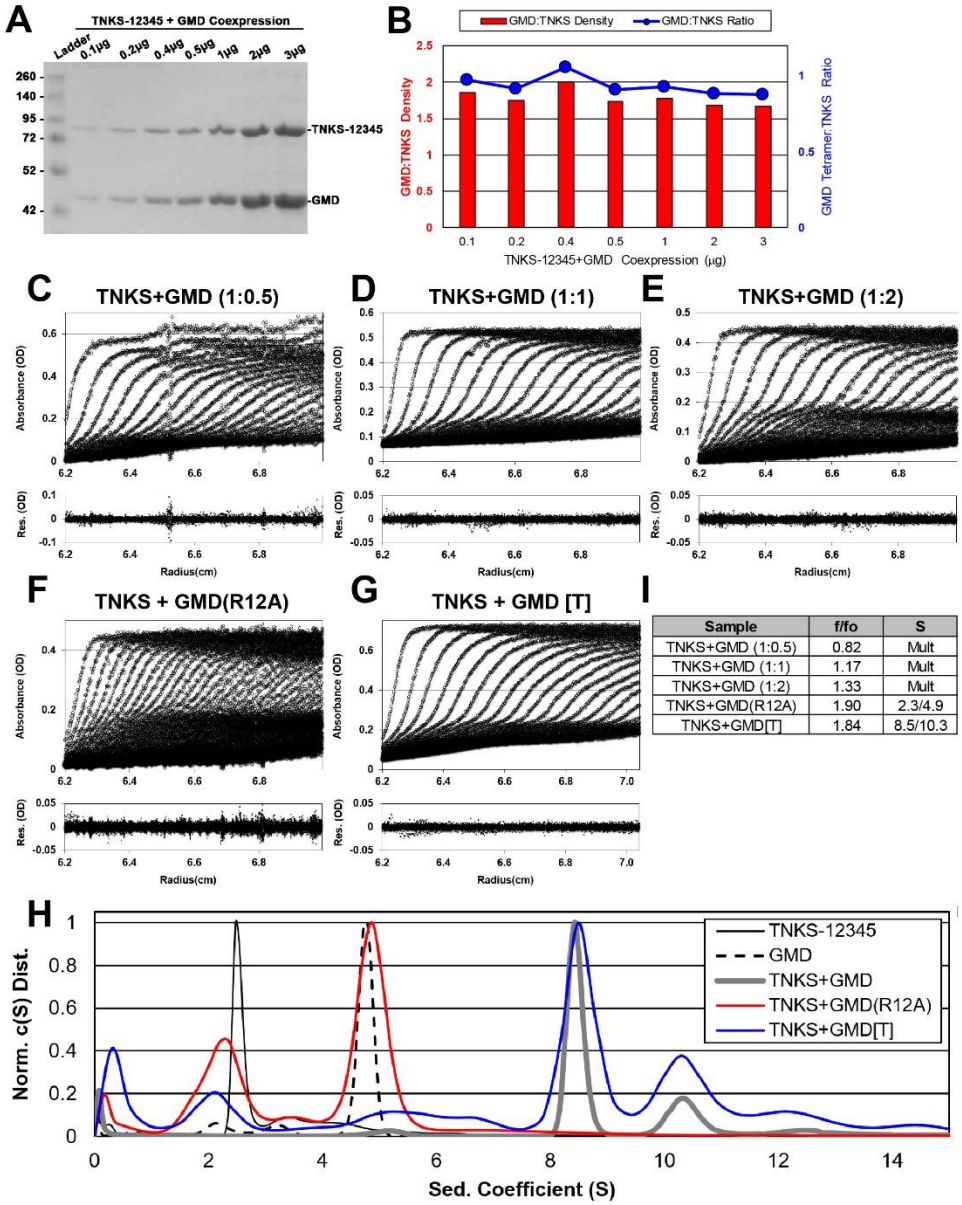

Figure S5. Analytical ultracentrifugation analysis of TNKS-12345 and GMD complexes. (A) Coomassie-stained SDS-PAGE of purified TNKS-12345 and GMD coexpression loaded at different concentrations. (B) Quantification of (A) depicting the ratio of GMD (167.8kDa tetramer) to TNKS-12345 (88.2kDa) (red bars, left vertical axis), and the apparent GMD tetramer:TNKS stoichiometry derived from that ratio (blue line, right vertical axis). Band density was determined using ImageJ. (C-E) Sedimentation velocity analysis of TNKS-12345 mixed with different ratios of GMD. The top panels show absorbance data (circle) and associated c(S) model fit (lines). The bottom panels show residuals for the fit. See Fig. 6F for c(S) distribution. GMD was maintained at 1.5 µM (tetramer concentration, 6 µM monomer) and TNKS-12345 was loaded at 3 µM (1:0.5 ratio), 1.5 µM (1:1) ratio, and 0.75 µM (1:2 ratio) for (C), (D), and (E) respectively. (F-H) Sedimentation velocity analysis (F,G) and c(S) distribution (H) of TNKS-12345 mixed with an equimolar concentration of GMD(R12A) (F) and GMD[T] (G). All proteins were loaded at 1.8 µM (tetramer concentration for GMD constructs) to achieve a 1:1 ratio. (I) Parameters derived from AUC analysis from (C-G).

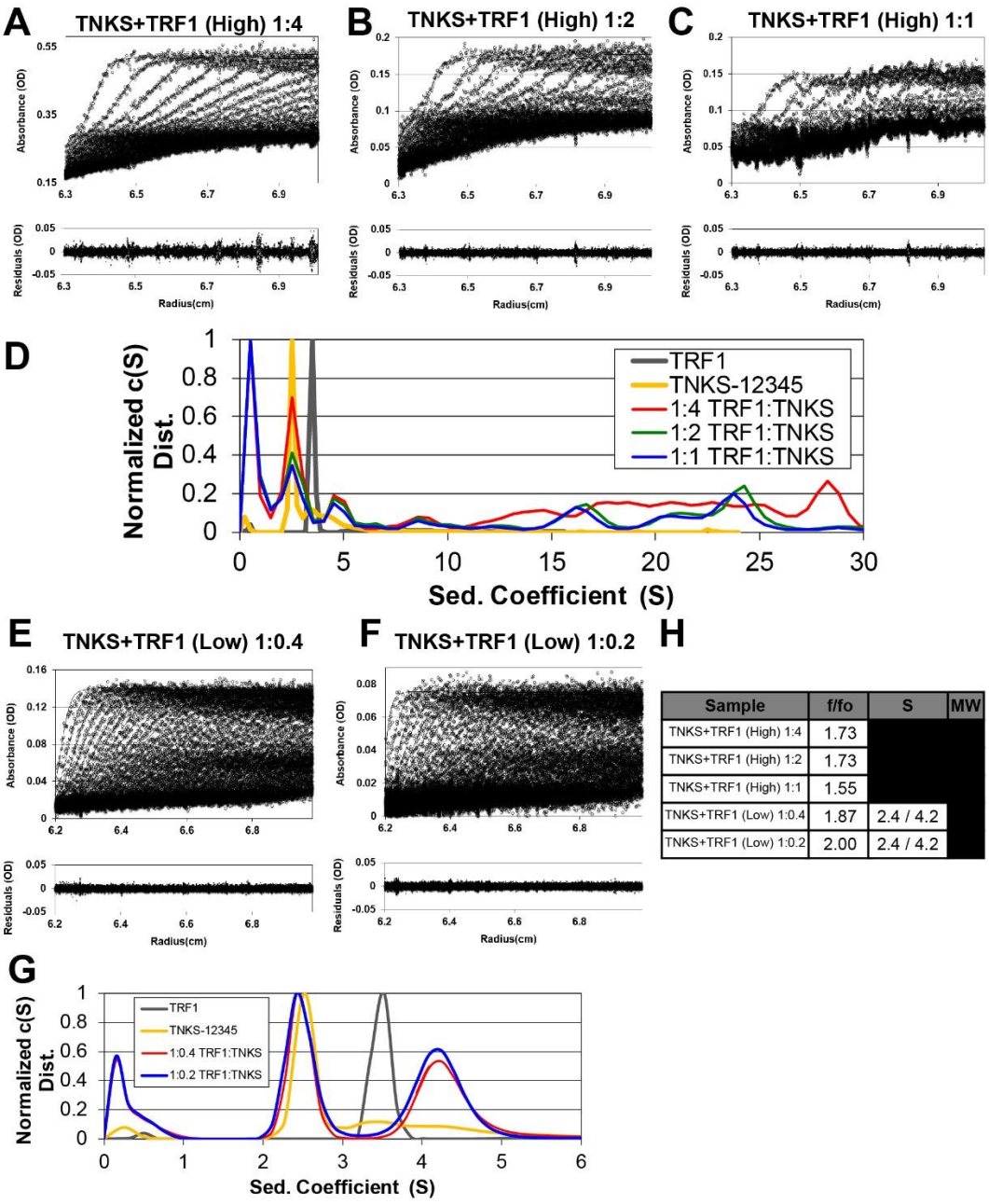

Sample	f/fo	S	MW
TNKS+TRF1 (High) 1:4	1.73		
TNKS+TRF1 (High) 1:2	1.73		
TNKS+TRF1 (High) 1:1	1.55		
TNKS+TRF1 (Low) 1:0.4	1.87	2.4 / 4.2	
TNKS+TRF1 (Low) 1:0.2	2.00	2.4 / 4.2	

Figure S6. Analytical ultracentrifugation analysis of TNKS-12345 and TRF1. (A-D) Sedimentation velocity analysis (A-C) and c(S) distribution (D) of TNKS-12345 mixed with TRF1 at "high" concentrations. In (A-C) TRF1 was maintained at 3.6 μM (dimer concentration, 7.2 μM monomer) and TNKS-12345 was loaded at 0.9 μM (1:4 ratio), 1.8 μM (1:2 ratio), and 3.6 μM (1:1 ratio) for (B), (C), and (D), respectively. (E-G). Sedimentation velocity analysis (E,F) and c(S) distribution (G) of TRF1 mixed with TNKS-12345 at "low" concentrations. TRF1 was maintained at 0.9 μM (dimer concentration, 1.7 μM monomer), and TNKS-12345 was loaded at 2.1 μM (1:0.4 ratio) and 4.1 μM (1:0.2 ratio) for (E) and (F) respectively. The top panels for (A-C,E,F) show absorbance data (circle) and associated c(S) model fit (lines). The bottom panels show residuals for the fit. (H) Parameters derived from AUC analysis from (A-G).

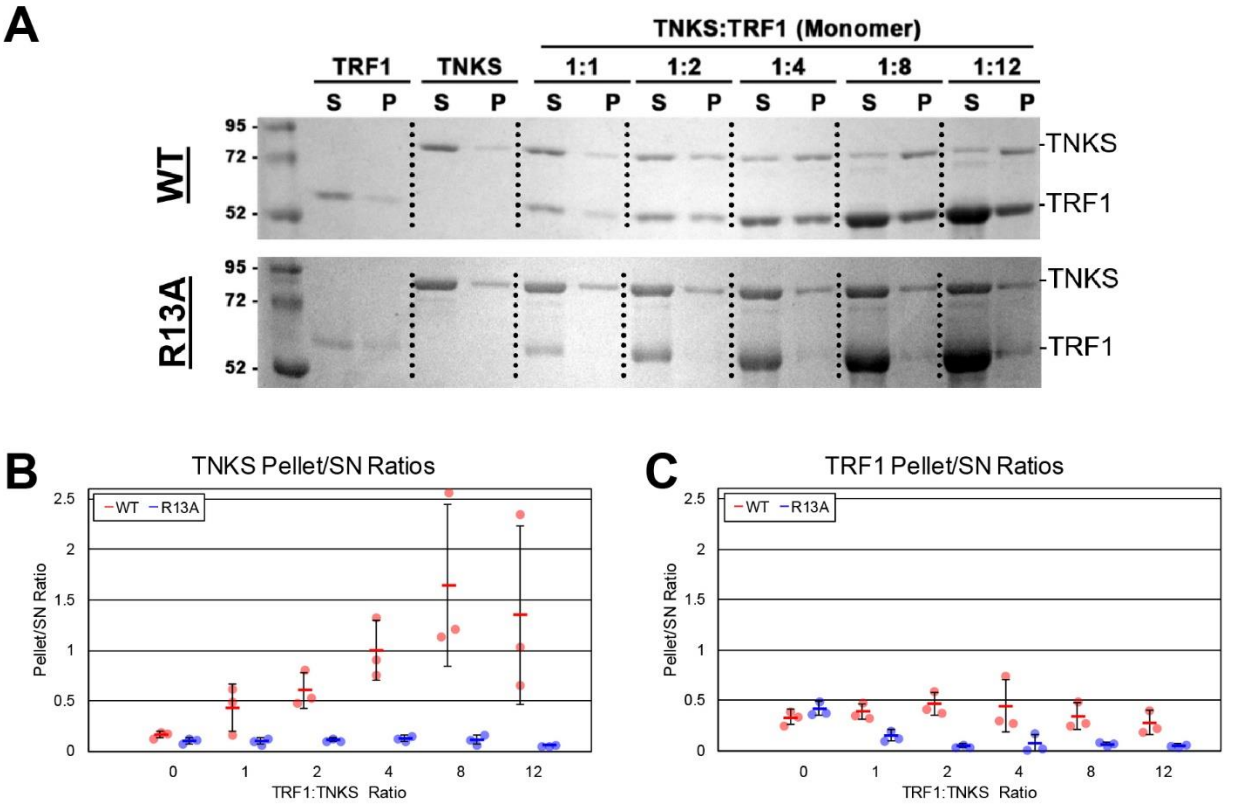

Figure S7. TNKS:TRF1 solubility assays. (A) Solubility assays measuring the effect of increasing TRF1 concentrations on the solubility of TNKS-12345. TNKS and TRF1 mixes were incubated for 30 minutes, and then spun down at top speed on a table top centrifuge for 10min. The supernatant (S) was removed, and the pellet (P) was resuspended in an equal volume, and all samples were evaluated by SDS-PAGE. TRF1 constructs used include wild type and non-binding TRF1(R13A). All ratios represent a monomer of TNKS-12345 and a monomer of TRF1. (B,C) Quantification of TNKS (B) or TRF1 (C) protein density in the supernatant and pellet, displayed as the pellet:supernatant ratio. Individual data points are depicted by circles, and averages are depicted by bars. Data represent mean ± standard deviation.

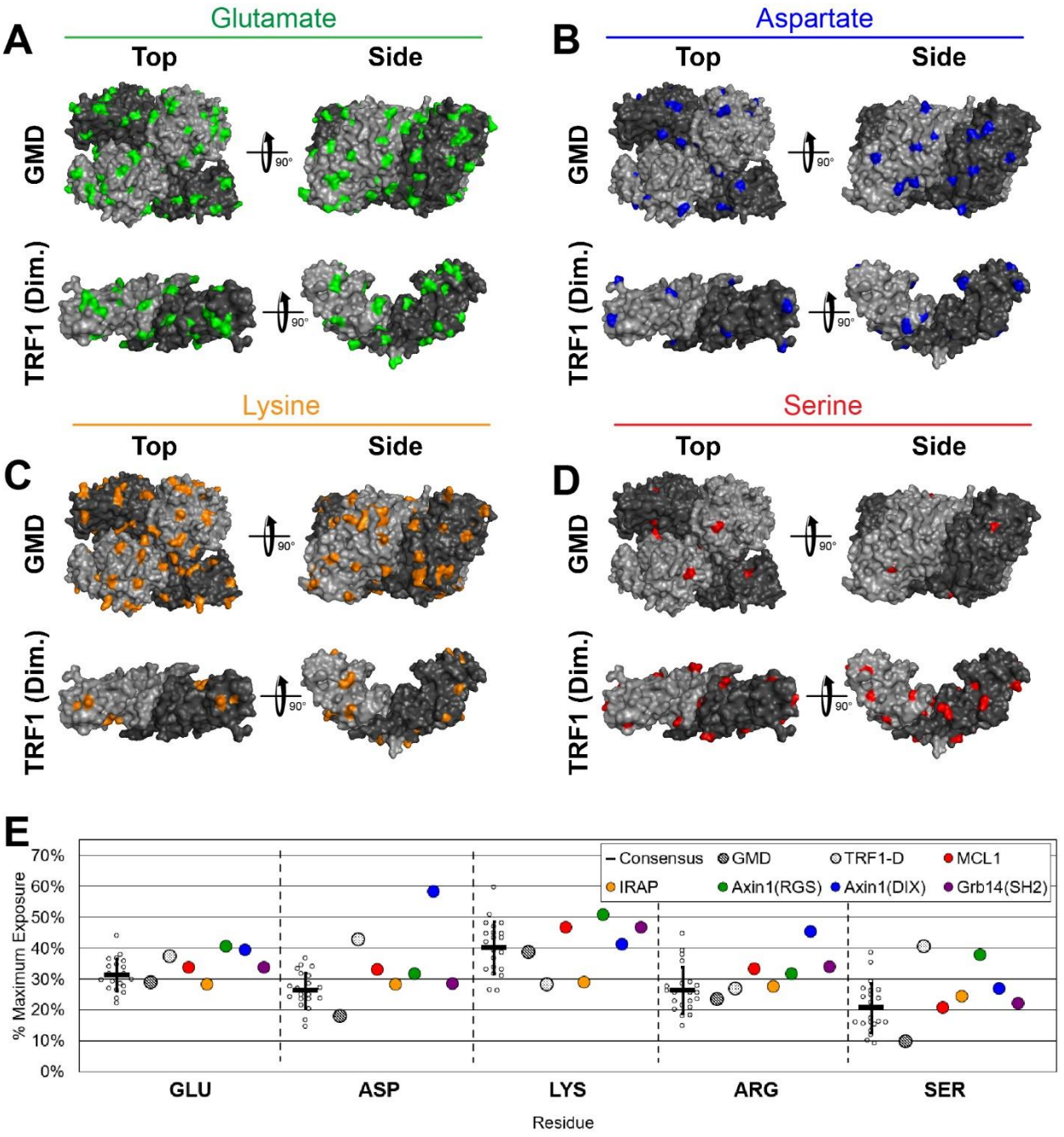

Figure S8. TNKS binding partner solvent accessibility. (A-D) Surface exposure of common PAR-accepting residues glutamate (A), aspartate (B), lysine (C), and serine (D) on the surface of crystal structures of the TRF1 dimerization domain (TRF1-D) (PDB # 1H6O) and GMD (PDB # 5IN5). (E) Solvent accessibility of crystal structures representing fragments of TNKS binding partners. Percent maximum exposure was determined as in Fig. 7A. See Table S1 for consensus structure library.

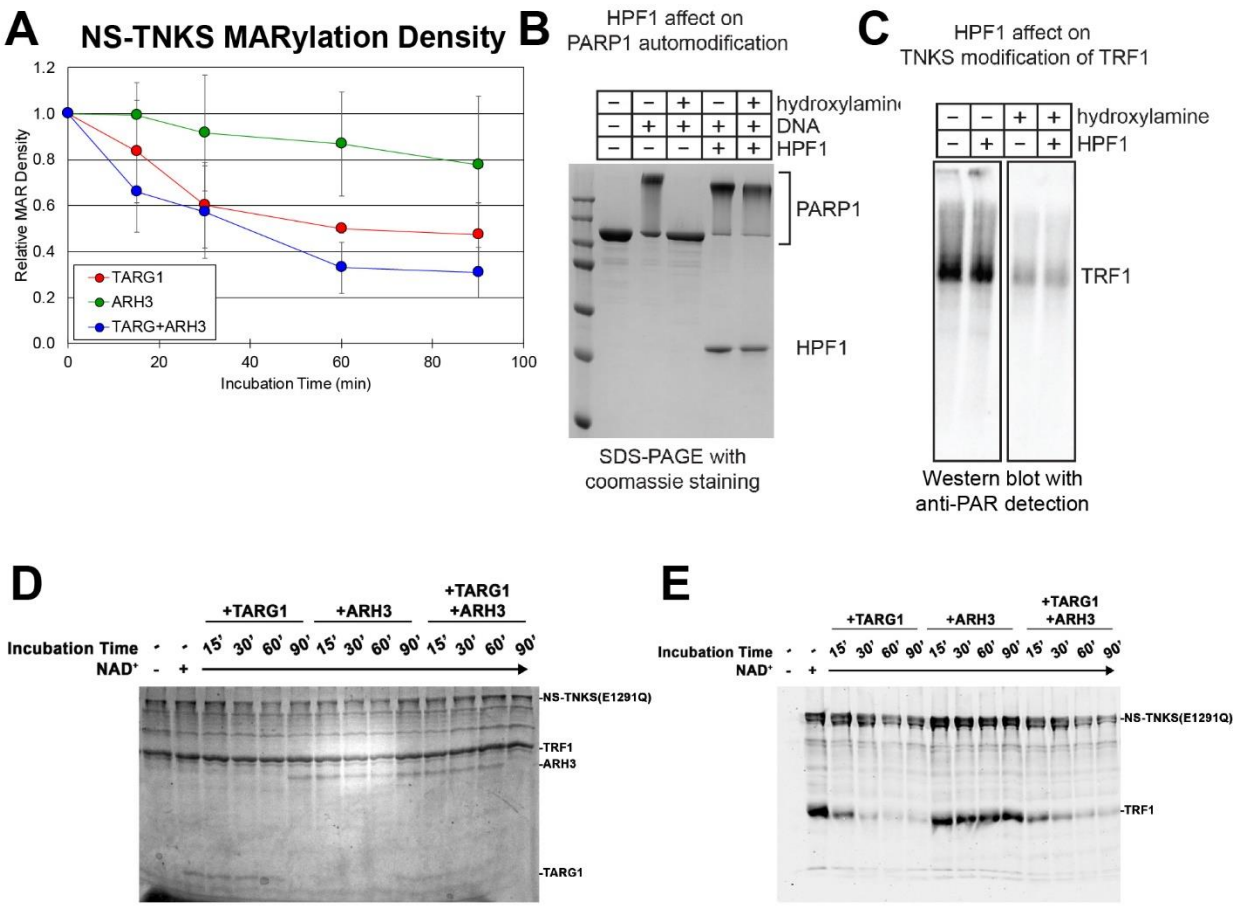

Figure S9. NS-TNKS MARylation density for hydrolase time series. (A) NS-TNKS MAR density as derived from Fig. 7D. Data represent mean ± standard deviation. (B) SDS-PAGE demonstrating the effect of HPF1 on PARP-1 residue targeting. In the absence of HPF1, automodified PARP-1 is sensitive to hydroxylamine treatment (lane 3), consistent with hydroxylamine-induced hydrolysis of the ester bond between glutamate/aspartate residues and ADP-ribose. In contrast, automodified PARP-1 is not sensitive to hydroxylamine hydrolysis in the presence of HPF1 (lane 5), suggesting that a different residue (serine) is targeted. (C) Western blot demonstrating the effect of HPF1 on TNKS and TRF1 ADP-ribosylation. The addition of HPF1 has no significant effect on either TNKS or TRF1 modification (lane 1 vs lane 2). The addition of hydroxylamine significantly reduces the TNKS and TRF1 ADP-ribose signal (lane 3), consistent with hydrolysis of modified glutamate/aspartate residues. This reduction is unaffected by the presence of HPF1 (lane 4), indicating that HPF1 does not influence TNKS residue targeting. (D and E) SDS-PAGE (D) and Western blot (E) for hydrolase time-series TNKS activity assay.

PDB	Macromolecule	GLU	ASP	LYS	ARG	SER	CYS
1A0L	BETA-TRYPTASE	66.3	60.5	119.8	78.8	41.5	5.1
1A7X	FKBP12	79.8	70.6	101.7	122.2	18	0
1D1S	ALCOHOL DEHYDROGENASE CLASS IV SIGMA CHAIN	69.3	47.8	113.4	63.9	24.4	6.2
1DGB	CATALASE	60.9	27.8	78.1	49.2	25	8.6
1EGC	MEDIUM CHAIN ACYL-COA DEHYDROGENASE	63.6	44.8	92.1	68.9	14.1	2.4
1FTA	FRUCTOSE-1,6-BISPHOSPHATASE	56.9	52.7	110.7	75.2	24.5	13.3
1H66	NAD(P)H DEHYDROGENASE [QUINONE] 1	59.8	50.6	105.1	107	24.1	0
1HW8	HMG-COA REDUCTASE	81.7	46.5	90	77.8	26.7	12.5
2A2Z	Deoxycytidine kinase	75.6	66	74.8	57.9	38.5	21.2
2A7R	GMP reductase 2	70.7	52.1	61.2	76.3	40.8	16.7
2AR9	Caspase-9	84.4	45.6	77.2	103.4	36.8	16.7
2GBT	Superoxide dismutase [Cu-Zn]	97.6	65.4	140.9	49.6	59.3	11
2GCG	Glyoxylate reductase/hydroxypyruvate reductase	70.5	59.9	105.3	97.8	23.3	8
2J91	ADENYLOSUCCINATE LYASE	58.6	40.9	86.5	62.4	37	5.6
2PSN	Alpha-enolase	49.4	32	101.6	54.5	40.5	2.2
3E04	Fumarate hydratase	52.8	55	73.1	40.6	15.4	0.6
4BKP	GDP-L-FUCOSE SYNTHASE	80.7	64.2	62.3	70.8	45	21.4
4QG6	Pyruvate kinase PKM	65.9	44.9	105.9	68.9	34.4	11.6
4RAB	Hypoxanthine-guanine phosphoribosyltransferase	64.9	51.7	79.3	69.9	54.7	0.1
4TNP	Deoxynucleoside triphosphate triphosphohydrolase SAMHD1	76.9	39.2	98.2	55.8	20.4	7.3
4WLE	Malate dehydrogenase, mitochondrial	74.9	47.4	112.7	61.4	24.6	3.7
1H6O	TRF1 Dimerization Domain	83.5	82.6	66.5	74	62.8	17
1T2A	GDP-mannose 4,6 dehydratase	64.4	34.7	91.4	64.4	15.2	13.1
5LOF	MCL1	75	63.2	109.5	91.3	32.1	0.1
5C97	IRAP	62.6	53.8	68.3	74.6	37.8	9.8
1DK8	Axin1 RGS Domain	89.8	61.2	119.7	86.2	58.5	24.4
1WSP	Axin1 DIX Domain (Rat)	87.6	112.3	97	123.3	41.1	99.8
2AUG	Grb14 SH2	75	54.9	110.1	93.1	33.9	11.7
	Maximum Surface Exposure (1)	223	193	236	274	155	167

Table S1. Solvent accessibility of consensus and TNKS binding partner crystal structures. Average residue exposure in consensus homomultimeric crystal structures and TNKS binding motif partners were determined using Surface Racer. Maximum exposure values represent the maximum theoretical solvent accessibility of individual residues in solution.

References

1. Tien, M. Z., Meyer, A. G., Sydykova, D. K., Spielman, S. J., and Wilke, C. O. (2013) Maximum allowed solvent accessibilites of residues in proteins. *PLoS One*. 10.1371/journal.pone.0080635